

The Virgo High-Resolution CO Survey: III. NGC 4254

Yoshiaki SOFUE,¹ Jin KODA,^{1,2} Hiroyuki NAKANISHI,¹ and Makoto HIDAKA¹

¹*Institute of Astronomy, The University of Tokyo, Mitaka, Tokyo 181-0015*

²*Nobeyama Radio Observatory, National Astronomical Observatory, Minamimaki, Minamisaku, Nagano 384-1305*
sofue@ioa.s.u-tokyo.ac.jp

(Received 2002 August 15; accepted 2002 October 15)

Abstract

We present high-angular-resolution ($1''.5$ – $5''$) interferometer observations of the ^{12}CO ($J = 1-0$) line emission in the central region of the SA(s)c galaxy NGC 4254 (M 99). The observations were obtained using the Nobeyama Millimeter-wave Array (NMA) during the course of a long-term CO-line survey of Virgo spirals. We present the spectra, channel maps, integrated intensity distributions, velocity fields, position–velocity diagrams, and compare the data with various optical images. The rotation velocity is already finite at the nucleus, or at least it rises steeply to 80 km s^{-1} within the central $1''$, indicating the existence of a massive core of $10^8 M_{\odot}$ within $1''$ (80 pc) radius. The CO intensity maps show that the inner disk has well-developed multiple spiral arms, winding out from a bar-shaped elongated molecular complex. In addition to the bisymmetric spiral arms, an asymmetric tightly wound arm with high molecular gas density is found to wind out from the molecular bar. The molecular spiral arms, particularly the tightly wound arm, well traces optical dark lanes, and are associated with $\text{H}\alpha$ arms having many H II regions. The inner asymmetric spiral structures can be explained by ram-pressure distortion of inter-arm low density regions of the inner disk by the intra-cluster gas wind, and is indeed reproduced by a hydrodynamical simulation.

Key words: clusters: individual (Virgo) — galaxies: individual (NGC 4254, M 99) — galaxies: ISM — galaxies: kinematics and dynamics — galaxies: spiral arms — ISM: molecular gas — ISM: ram pressure

1. Introduction

The Virgo member spiral NGC 4254 (M 99) is an SA(s)c galaxy (RC3) with an optical radius of $5'.36$ (de Vaucouleurs et al. 1991), and an inclination angle of 42° (Phookun et al. 1993). We adopted the Cepheid calibrated distance of 16.1 Mpc of the Virgo Cluster for this galaxy (Ferrarese et al. 1996), with which the Tully–Fisher distance of 16.8 Mpc is consistent (Schöniger, Sofue 1997). The parameters of the galaxy are given in table 1.

Optical images show that the galaxy is dominated by a three-arm structure, exhibiting $m = 1$ and $m = 3$ modes (Iye et al. 1982; González, Graham 1996). This one-armed structure is also seen in the H I gas distribution (Phookun et al. 1993). Such an asymmetric spiral pattern is often observed in tidally interacting galaxies, but there is apparently no massive companion around NGC 4254. Moreover, a tidal interaction generally produces a bisymmetric structure with near and far side arms, and the resultant spiral structure shows $m = 2$ mode features, but not the $m = 1$ or $m = 3$ mode. Therefore, the asymmetric spiral pattern of NGC 4254 would be due to some other mechanisms, such as an interaction with the intracluster medium (ICM), as suggested by the H I head–tail structure.

It is an interesting question as to how deeply the ICM ram effect can affect the galactic disks and whether the molecular disks are indeed disturbed. In fact, Hidaka and Sofue (2002) have shown by a numerical simulation that a ram effect by ICM wind can produce lopsided molecular arms in the central few kpc region, if the inter-arm gas density is low enough even though the mean radial density is high enough to avoid the ram effect. In such a circumstance, the ICM ram pressure

perturbs the orbits of the low-density inter-arm gas, which results in significantly displaced shocked arms from unperturbed arms.

In this paper, we present high-resolution ^{12}CO ($J = 1-0$) line observations of NGC 4254 using the Nobeyama mm-wave Array (NMA) in AB, C, and D array configurations. The observational parameters and detailed procedures are described in the first paper of this series, reporting the high-resolution CO line Virgo survey (ViCS: Sofue et al. 2003a). We discuss the kinematics and ISM properties based on the CO data, and compare the result with various optical images. Environmental effects, such as the tidal interaction and/or the ram-pressure effects, would be an interesting subject for some Virgo galaxies located near to the cluster center and moving in the dense intra-cluster medium. Based on the CO data, we discuss the possibility that the distribution and kinematics of molecular clouds in the central region can be affected by the ram-pressure effect of the intracluster medium.

2. Observations

^{12}CO ($J = 1-0$) high-angular-resolution interferometer observations of the central region of NGC 4254 were carried out on 2000 March 10–11, 2000 February 4–5, and 1999 December 8, using the Nobeyama Millimeter Array (NMA) in the AB, C, and D configuration, respectively. Table 2 gives the observational parameters. Each observation run took typically 8 hours, including calibrations. The pointing center was at R.A. (J2000) = $12^{\text{h}}18^{\text{m}}50^{\text{s}}.03$, Dec. (J2000) = $+14^{\circ}24'52''.8$, adopted from Condon et al. (1990). However, this position was found to be $5''.9$ to the east and $6''.3$ to the south of the

Table 4. Parameters of maps.[†]

Resolution	Weighting	Beam		Velocity		r.m.s. noise	T_b for
		FWHM (arcsec)	P.A. (deg)	Resolution (km s^{-1})	Sampling (km s^{-1})	σ (mJy beam^{-1})	1 Jy beam^{-1} (K)
Low	Taper	5.22×3.45	152.0	21.0	10.5	19.6	5.1
Medium	Natural	2.99×2.34	148.0	21.0	10.5	15.4	13.2
High	Uniform	1.67×1.53	167.5	21.0	10.5	21.3	36.0

[†] The map centers are set at the derived dynamical center: $(\alpha_{2000}, \delta_{2000}) = (12^{\text{h}}18^{\text{m}}49^{\text{s}}609, +14^{\circ}24'53''.1)$.

Table 1. Properties of observed galaxies.

Morphology ¹	SA(s)c
NED position ² (J2000)	$\alpha = 12^{\text{h}}18^{\text{m}}49^{\text{s}}56$ $\delta = +14^{\circ}24'59''.4$
Apparent magnitude ¹	10.44
Systemic velocity ¹	2407 km s^{-1}
Inclination angle ³	42°
Position angle ³	68°
Assumed distance ⁴	16.1 Mpc ($1'' = 78.06 \text{ pc}$)

References: 1. de Vaucouleur et al. (1991); 2. NASA Extragalactic Database (<http://nedwww.ipac.caltech.edu/>); 3. Phookun et al. (1993); 4. Ferrarese et al. (1996).

Table 2. Observation Parameters.

Observed center frequency	114.353 GHz
Array configurations	AB, C, and D
Observing field center (Condon et al. 1990):	
α (J2000)	$12^{\text{h}}18^{\text{m}}50^{\text{s}}03$
δ (J2000)	$+14^{\circ}24'52''.8$
Derived dynamical center:	
(assumed to be nucleus position \simeq map center in this paper)	
α (J2000)	$12^{\text{h}}18^{\text{m}}49^{\text{s}}61$
δ (J2000)	$+14^{\circ}24'59''.1$
Central velocity	2400 km s^{-1}
Frequency channels	256
Total bandwidth	512 MHz
Velocity coverage	1342 km s^{-1}
Velocity resolution	5.24 km s^{-1}
Amplitude and phase calibrator	3C 273
Primary beam	$65''$
Cell size	$0''.25$

Table 3. Comparison of our center position with other observations.

R.A. (J2000)	Dec. (J2000)	References
$12^{\text{h}}18^{\text{m}}49^{\text{s}}61$	$+14^{\circ}24'59''.1$	CO: This work
$12^{\text{h}}18^{\text{m}}49^{\text{s}}63$	$+14^{\circ}24'58''.8$	CO: Sakamoto et al. (1999)
$12^{\text{h}}18^{\text{m}}49^{\text{s}}43$	$+14^{\circ}24'59''.5$	<i>B</i> -band photometry: Yasuda et al. (1995)
$12^{\text{h}}18^{\text{m}}49^{\text{s}}73$	$+14^{\circ}24'58''.8$	IRAS: Soifer et al. (1987)

newly determined kinematical center of the galaxy using our high-resolution CO-line velocity field. In this work, therefore, we adopted the new kinematical center as our origin of the maps, whose coordinates are R.A. (J2000) = $12^{\text{h}}18^{\text{m}}49^{\text{s}}61$ and Dec. (J2000) = $+14^{\circ}24'59''.1$. The present center position may be compared with the other observations listed in table 3, which all coincide within $\sim \pm 0''.5$.

We also observed nearby radio point source 3C 273 as a flux and phase calibrator every 20 min. Because the intrinsic flux density of 3C 273 at the observing frequency was non-periodically variable, we performed flux calibration for each observation. The flux density of 3C 273 was 11.25, 12.40, and 11.26 Jy, in the observations of the AB, C, and D configurations, respectively. We used a spectro-correlator system, Ultra Wide Band Correlator (UWBC: Okumura et al. 2000) in a narrow-band mode, which had 256 channels; the total bandwidth was 512 MHz. One channel corresponded to 5.24 km s^{-1} at the observing frequency.

The raw data were calibrated using UVPROC-II, a first-stage reduction system developed at the Nobeyama Radio Observatory (NRO), and were then Fourier-transformed using the NRAO Astronomical Image Processing System (AIPS). We reduced the thus-obtained dirty map by the CLEAN method using three different weighting functions and tapering, as summarized in table 4.

First, we obtained low-resolution maps using a natural weighting function, tapered by a Gaussian function having deviations of $60 \text{ k}\lambda$ and a cut-off at greater than $80 \text{ k}\lambda$ in (u, v) space. The data were averaged in 4 bins, yielding a 128-channel data cube with a velocity resolution of 21 km s^{-1} ; the channel increment was 2, corresponding to 10.4 km s^{-1} . The synthesized beam was $5''.22 \times 3''.45$, and the obtained channel had a typical r.m.s. noise of $19.6 \text{ mJy beam}^{-1}$.

Second, we obtained the most representative maps from the present observations using a natural weighting function, no taper. The data were averaged in 4 bins (21 km s^{-1}) of the original channels, and the channel increment was 2 (10.4 km s^{-1}), yielding a 128-channel data cube. The synthesized beam was $2''.99 \times 2''.33$, and the typical r.m.s. noise on a channel map was $15.4 \text{ mJy beam}^{-1}$.

Third, we obtained high-resolution maps, using a uniform weighting function, no taper. The data were averaged in 2 bins giving a velocity resolution of 10.4 km s^{-1} ; the channel increment was 2 (10.4 km s^{-1}). The synthesized beam was $1''.67 \times 1''.53$, and the typical r.m.s. noise was $21.3 \text{ mJy beam}^{-1}$.

3. Results

3.1. Spectra

Figures 1a and b show CO line spectra averaged in a $1' \times 1'$ squared region (4.89 kpc square) around the center and a $20'' \times 20''$ squared region (1.69 kpc square), respectively. Both spectra indicate double horn shapes, typical for a rotating disk. However, the central spectrum in figure 1b has a much narrower width, $\sim 130 \text{ km s}^{-1}$, than that of the outer region, where the width is 210 km s^{-1} . Since the double-horn feature is typical for a rotating disk with a constant rotation velocity, the clearly different velocity widths suggest that the disk rotation velocity varies step-like at a few kpc from the center, which is discussed in a more detail using position–velocity diagrams in a later section.

Figure 1c shows a CO line spectrum of NGC 4254 obtained by convolution with a synthesized Gaussian beam of FWHM $45''$ in order to compare the present CO intensity with that of the FCRAO 14-m single-dish observation (Kenney, Young 1988). Here and throughout this paper, no primary beam correction has been applied. The peak intensity and the integrated intensity of our NMA observation are $2.39 \text{ Jy Beam}^{-1}$ and $325.58 \text{ Jy Beam}^{-1} \text{ km s}^{-1}$, corresponding to 106 mK and 14.8 K km s^{-1} , respectively. A FCRAO CO observation of NGC 4254 shows that the peak intensity is $89/\eta_B \text{ mK}$, and the integrated intensity is $(10.6 \pm 2.0)/\eta_B \text{ K km s}^{-1}$, where η_B is the beam efficiency of the FCRAO 14 m telescope, which is equal to 0.53 ± 0.04 . Hence, the integrated intensity of our NMA observation covers 74% of the integrated intensity of the FCRAO single-dish observation.

3.2. CO Intensity Maps

Figure 2 shows channel maps at a velocity separation of 10.4 km s^{-1} . Each channel map displays an averaged brightness in a 21 km s^{-1} velocity range. The CO emission is visible from the 6th channel at $V_{\text{lsr}} = 2300 \text{ km s}^{-1}$ to the 27th channel at 2517 km s^{-1} . The distributions in individual channel maps are generally along iso-velocity lines, typical for a rotating disk galaxy, while they are patchy, indicating that the distribution is not uniform, but concentrated in the arms.

Figure 3 shows the total CO intensity map at a low resolution of $5''.22 \times 3''.45$. Figure 4a shows the total CO intensity map at the representative resolution of $2''.33 \times 2''.99$ using a natural weighting function. The major and minor axes across the dynamical center are shown by the big crosses in figures 3 and 4a. Figure 5a shows the same view but at the highest resolution of $1''.67 \times 1''.53$ with uniform weighting.

3.2.1. Central CO bar

The CO emission shows an elongated bar-like concentration around the map center (kinematical center) with the major axis at a P.A. of about 50° , being displaced from the galaxy's major axis at P.A. = 68° . The center of gravity of this bar is slightly offset from the kinematical center toward the north. Although the CO distribution shows a bar feature, the optical morphology is non-barred SA(s)c type (RC3). In fact, no bar feature is recognized in either the *R*-band image shown in figure 6a or in *K*-band image in figure 8, as is shown later.

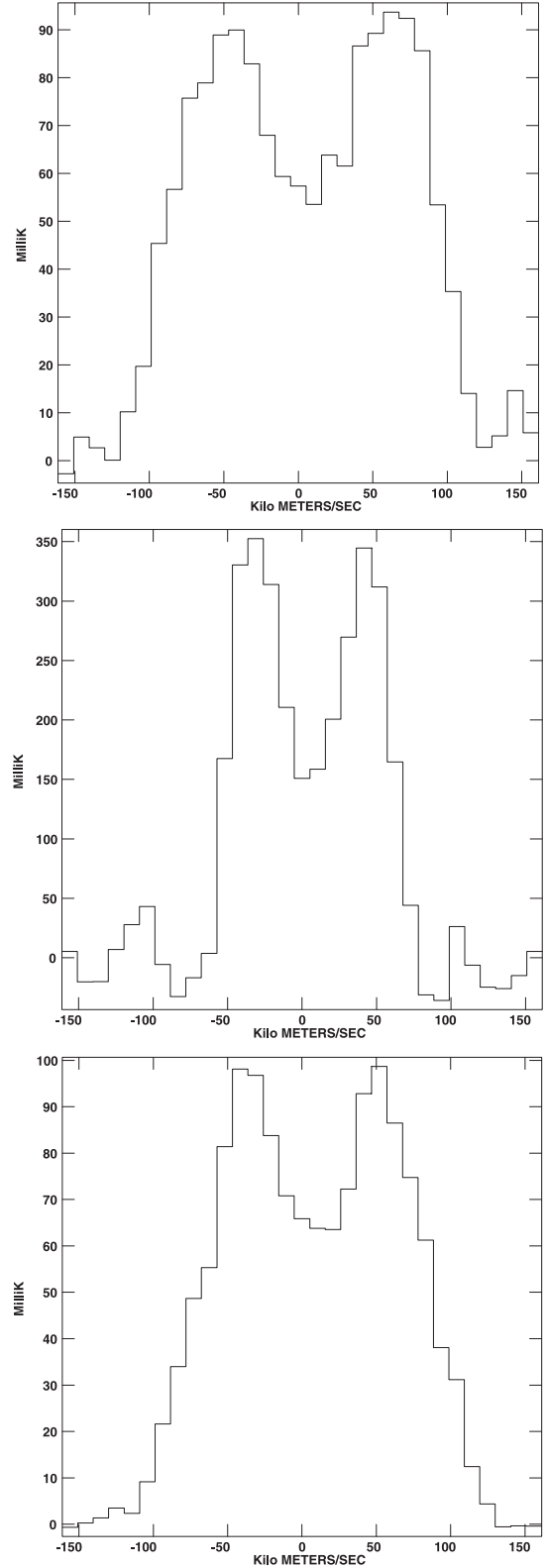


Fig. 1. (a) (Top:) Spectrum averaged in the central $60''$ squared area, showing a double-horn shape indicative of a rotating disk. (b) (Middle:) Spectrum averaged in the central $20''$ squared area, showing a double-horn shape, but with a much narrower width than in figure 1a, indicative of a rotating disk at a slower velocity. (c) (Bottom:) Spectrum at the center after convolved with a Gaussian beam of FWHM $45''$.

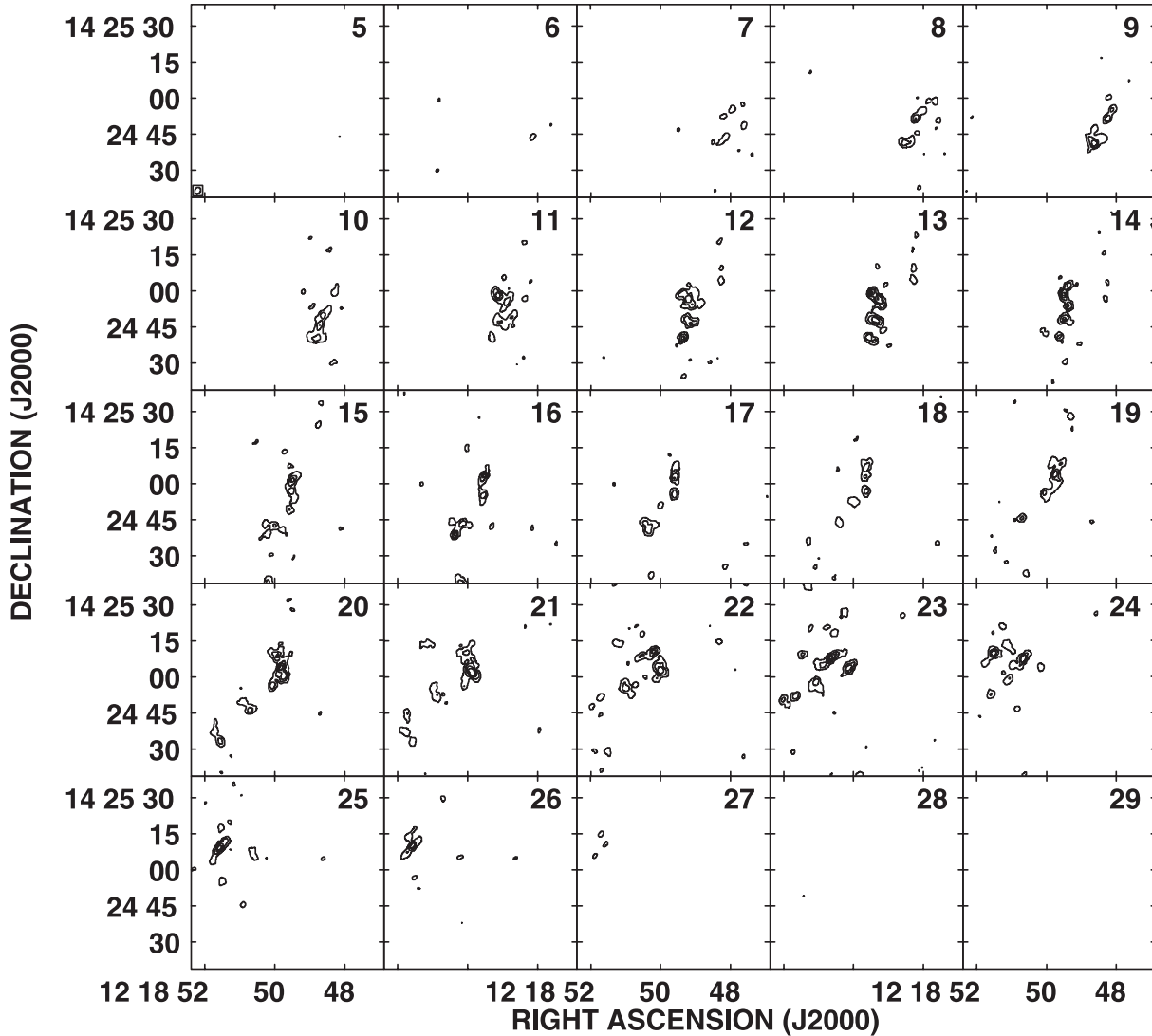


Fig. 2. Channel maps of the CO-line intensity at a 10.4 km s^{-1} velocity increment, each indicating the CO-line intensity integrated in a 21 km s^{-1} velocity range. The 10th, 15th, and 20th channels correspond to $V_{\text{lsr}} = 2340.2, 2392.6,$ and 2444.2 km s^{-1} , respectively. The intensity unit is the brightness temperature in K. Contours are drawn at every 20% of the peak intensity of 3.93 K .

3.2.2. *Spiral arms*

Two major spiral arms are winding out from both ends of this central molecular bar in an counterclockwise direction, and extend until the field edge. In figure 3 we name the western major arm Arm I, and the eastern major arm Arm II. At R.A. = $12^{\text{h}}18^{\text{m}}51^{\text{s}}.5$, Dec. = $14^{\circ}24'10''$ (J2000), there is a segment of an arm-like feature with a dense molecular complex, running parallel to Arm II.

3.2.3. *Tightly wound arm*

Soon after it starts from the eastern end of the central CO bar, Arm II bifurcates into a more tightly wound dense arm, which we call Arm III, as indicated in figure 3. The western end of this tightly-wound arm runs closely parallel to Arm I, as is more clearly seen in figures 4a and 5a. This tight arm has a much higher brightness, about twice to three times that of the two major spiral arms.

3.2.4. *North–South asymmetry*

The global distribution of molecular gas in the observed region of NGC 4254, as shown in figures 3 to 5, is highly asymmetric with respect to the major axis. The southern half is much CO brighter compared to the northern half. Most of the asymmetry comes from the tight CO arm, Arm III.

3.3. *Velocity Field*

Figure 4b shows an intensity-weighted velocity field corresponding to figure 4a with natural weighting, and figure 4c is an overlay of the same velocity field on the integrated intensity map at a lower resolution in the gray scale, which is the same as figure 3. Figure 5c shows the velocity field for the central region at high resolution, corresponding to figure 5b. Figure 5d enlarges the central $4''$ region of figure 5c.

We determined the kinematical center as the position where the iso-contours run most tightly in the high-resolution velocity field in figures 5c and d: R.A. (J2000) = $12^{\text{h}}18^{\text{m}}49^{\text{s}}.61$ and

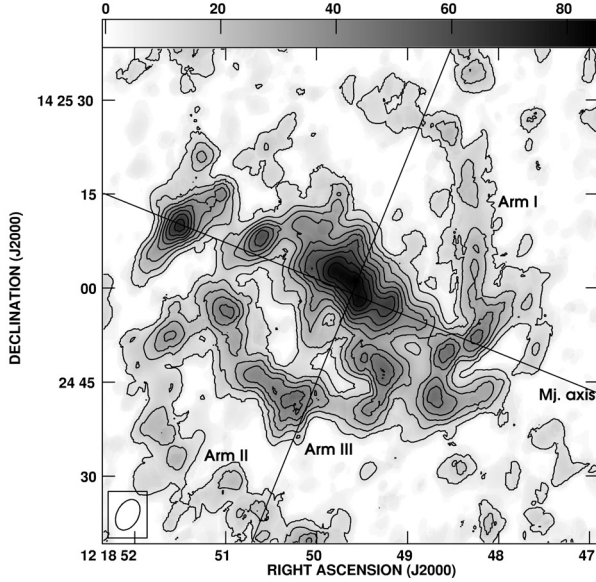


Fig. 3. Integrated CO-line intensity map (the zero-th moment map) of NGC 4254. The uv weighting function is natural, and tapered. The synthesized beam is $5''.22 \times 3''.45$ (P.A. = 152°). The contour levels are every 10% of the peak intensity of 85.2 K km s^{-1} ($16.6 \text{ Jy beam}^{-1} \text{ km s}^{-1}$). The major and minor axes are indicated by the cross.

Dec. (J2000) = $+14^\circ 24' 53''.1$ with an accuracy of $\pm 0''.3$. We adopt these coordinates as the center position of the galaxy, and assume that the position coincides with the nucleus. These coordinates are in accordance with the dynamical center determined by applying the task GAL in the AIPS reduction package, which uses a Brandt rotation curve to fit the (R.A., Dec., Velocity) cube. The fitted result to the entire disk in the observed area was R.A. (J2000) = $12^{\text{h}} 18^{\text{m}} 49^{\text{s}} 56$ and Dec. (J2000) = $+14^\circ 24' 58''.5$. The GAL fitting also gave the position angle of the molecular disk to be P.A. = 66.5° , inclination 38.8° , and the systemic velocity 2403.6 km s^{-1} , which are consistent with the adopted parameters in table 1.

The general pattern of the velocity field in figure 4b shows a symmetric spider diagram, indicating a regular circular rotation of the CO disk, with the eastern half red-shifted and the western half blue-shifted. Assuming that the spiral arms are trailing, the rotation is clockwise and, accordingly, the northern side is the near side. On smaller scales, the non-circular velocity components are superimposed. Individual spiral arms show iso-velocity contours running obliquely to those expected from a circular rotation, indicating non-circular streaming motion due to spiral density waves.

The central CO bar, whose major axis is at about P.A. = 50° , is rotating rather circularly with the node of the velocity field coinciding with that of the P.A. of the galaxy at 68° . However, the very central region within $2''$ from the nucleus is superposed by non-circular motion, where the iso-velocity contours run in an integral-sign shape with their average direction in the north-south, and the velocity node is at P.A. = 80° , significantly displaced from the galaxy's major axis.

3.4. Overlays on Optical Images

In figure 6a we overlay our CO intensity contour map at medium resolution (figure 4a) on a g -band image from the Princeton Galaxies Catalogue obtained with the Palomar 1.5-m telescope by Frei et al. (1996). The kinematical center was assumed to coincide with the optical nucleus. Scaling and positioning are accurate within an error of about $2''$, which applies to all the following overlays. Figure 6b shows the same region, but superposed on a 5957 \AA -band image from the HST WFPC2 archive. Figure 6c shows the central region with the high-resolution CO contour map on the HST image as in figure 6b. The CO arms, particularly the tightly-wound dense CO arm (Arm III), well trace the optical dust lanes running along the inner sides of the optical spiral arms. An inner dust lane at about $6''$ south-east of the nucleus is also traced by a CO arm, starting from the eastern mid-point of the central CO bar. Inside the CO bar, most of the CO clumps are generally associated with dust lanes and/or dusty clumps. However, the molecular bar, itself, does not well draw an overall spiral pattern, whereas the HST optical image within $10''$ of the nucleus shows symmetric amorphous spiral patterns.

Figure 6d shows an overlay of a medium-resolution CO map on a negative $H\alpha$ image taken from the NED archive of a survey of H II regions in spiral galaxies obtained by Banfi et al. (1993) using the 2.1-m KPNO telescope. This figure demonstrates an excellent global correlation of molecular arms and clouds with H II regions, indicating that star formation occurs in spiral arms with dense molecular clouds. A more detailed inspection of figure 6d reveals, however, that some intense molecular clouds are not directly superposed on H II regions, but are slightly displaced from the star-forming region. Also, some strongest H II regions are not superposed by CO clumps, but are slightly shifted from molecular cloud centers. The displacement generally occurs in the direction perpendicular to the arms in the sense that the H II regions are located outside of the CO arms (dark lanes). This is reasonably explained by the galactic shock-wave theory. However, the displacement also occurs among H II regions and molecular clumps along the arms. This fact shows that intense molecular clouds are places where star formation has not yet started. On the other hand, the strongest H II regions have already exhausted their parent molecular clouds.

3.5. PV Diagram

The position-velocity (PV) diagrams along the major axis at P.A. = 68° crossing the nucleus of NGC 4254 are shown in figures 7a to c in the order of low, medium, and high resolutions, respectively. The slit widths are $10''$, $3''$, and $2''$, respectively. Figure 7c enlarges the central part.

Emission in the PV diagram is separated into two major concentrations around the nucleus at finite velocity offsets of about $\pm 40 \text{ km s}^{-1}$ from the systemic velocity. The PV diagram shows a clear intensity minimum at the nucleus, which is prominent in figure 7c, despite the continuous distribution of CO emission in the integrated intensity maps (figures 3 to 5). This indicates that the rotation velocity rises very steeply within the central $1''$ or less.

After attaining the intensity maximum in the PV diagram,

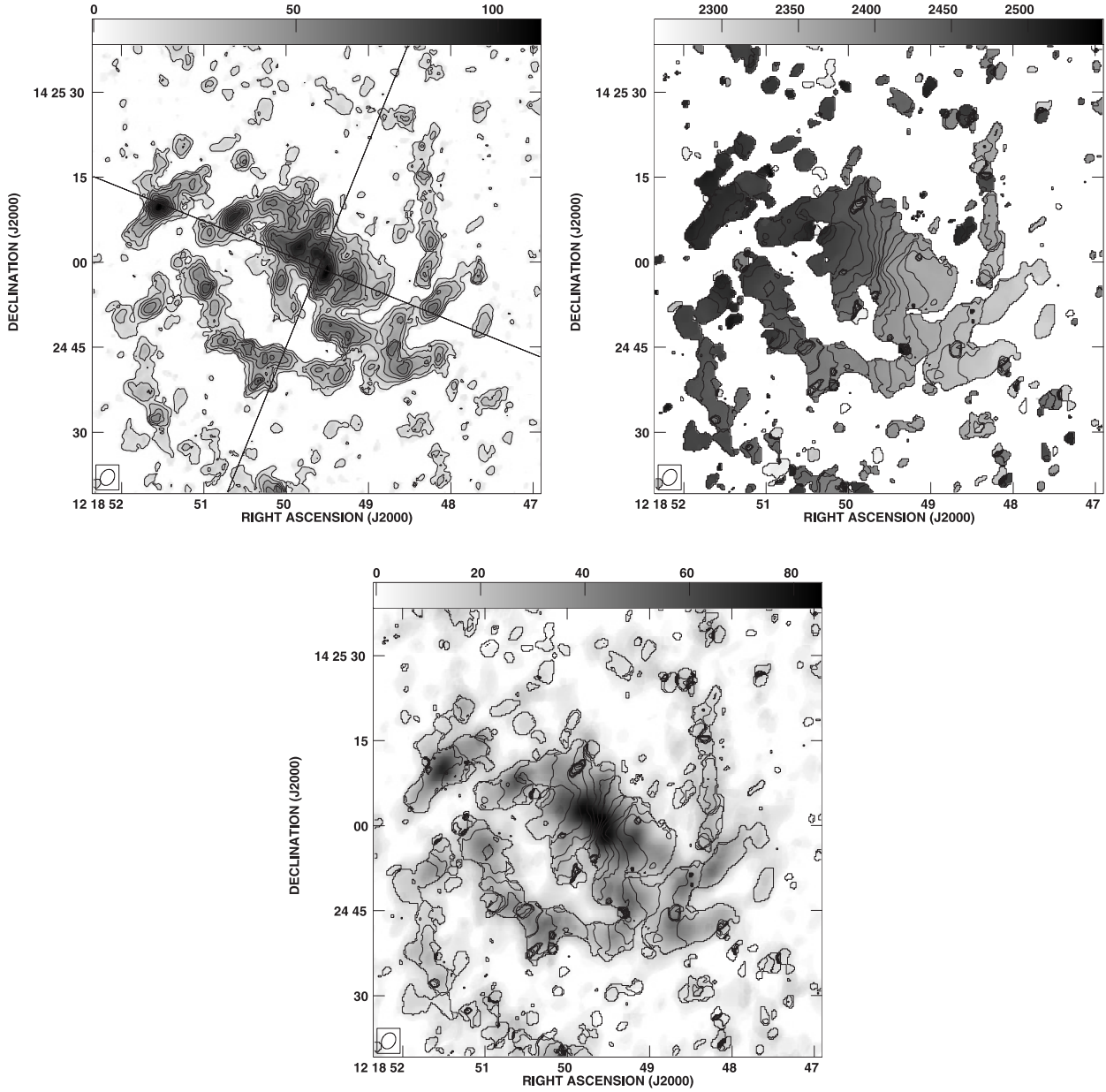


Fig. 4. (a) (Top left:) Integrated CO intensity map. The uv weighting function is natural, and non-tapered. The synthesized beam is $2''.99 \times 2''.34$ (P.A. = 148°). The central cross indicates the dynamical center and the major and minor axes. Because the attenuation due to the primary beam pattern is not corrected, the noise level is uniform in this image. The contour levels are every 10% of the peak flux of $110.3 \text{ K km s}^{-1}$ ($8.33 \text{ Jy beam}^{-1} \text{ km s}^{-1}$). The r.m.s. noise in the map is $1\sigma = 388 \text{ mJy beam}^{-1} \text{ km s}^{-1}$. (b) (Top right:) Velocity field of NGC 4254 (first moment map) corresponding to figure 4a. The synthesized beam is equal to that of figure 4a. The interval of the iso-velocity contours is 10 km s^{-1} . (c) (Bottom:) Overlay of the velocity field on the low-resolution intensity distribution from figure 3 in gray.

the velocity increases more gently toward the edges of the bar. Near the ends of the bar, the PV velocity increases step-like, and attains maximum velocities of about $\pm 100 \text{ km s}^{-1}$ in the spiral arms.

4. Discussion

4.1. Rotation Curve and Dynamical Mass

The inclination angle of NGC 4254 was obtained to be $i = 42^\circ$ from HI data (Phookun et al. 1993). Figure 8 shows a contour-form K -band image taken from NED data archive of

the near-IR surface photometry of spiral galaxies (Möllenhof, Heidt 2001). We determined the inclination angle by an ellipse fit to the iso-intensity contours of the K -band image, and obtained an inclination angle of $i = 42^\circ (\pm 1^\circ)$, consistent with the earlier value. We adopted this inclination angle in the present work. On the other hand, more face-on values have been obtained from CO observations: 29° (Sakamoto et al. 1999) or 28° (Kenney, Young 1988). Our CO maps, representing the two open spiral arms, also suggest a more face-on value. However, we may rely more on the inclinations from NIR images, because the CO maps manifest spiral-shocked gaseous

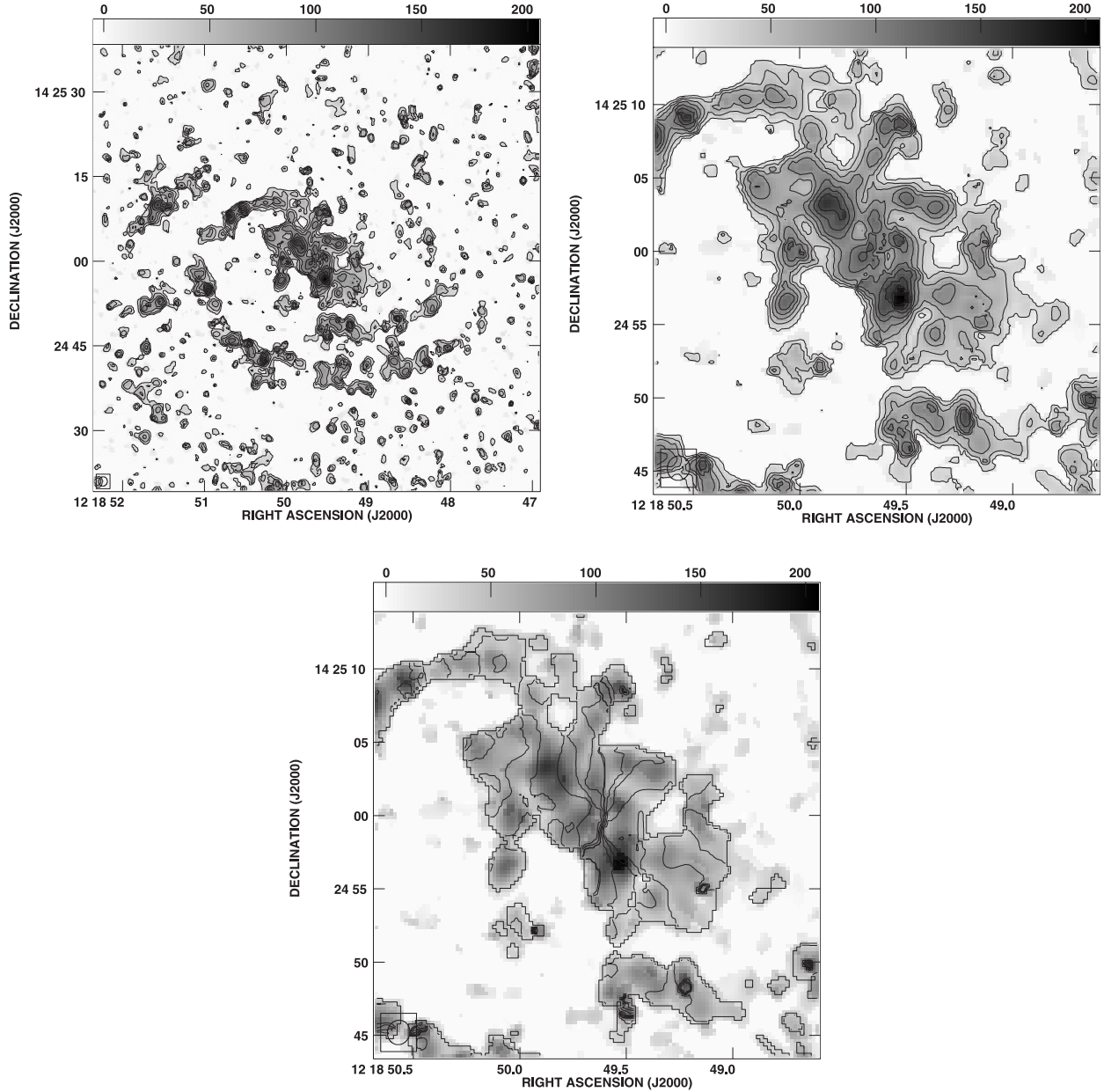


Fig. 5. (a) (Top left:) Integrated CO intensity map of NGC 4254, with uniform weighting. The synthesized beam is $1''.68 \times 1''.53$ (P.A. = $167^\circ.5$). The contour levels are every 10% of the peak flux of $205.3 \text{ K km s}^{-1}$ ($5.694 \text{ Jy beam}^{-1} \text{ km s}^{-1}$). (b) (Top right:) Enlargement of the central part of figure 5a. The beam size and contour intervals are the same as figure 5a. (c) (Bottom:) Velocity field of NGC 4254 (first moment map) corresponding to figure 5a. The synthesized beam is equal to that of figure 5a. The interval of the iso-velocity contours is 10 km s^{-1} .

arms, but not necessarily the backbone stellar disk.

We used PV diagrams to obtain a rotation curve by applying an iteration method developed by Takamiya and Sofue (2002) and Sofue et al. (2003b). Figure 9a shows the obtained rotation curve with an inclination angle of 42° being corrected. The rotation velocity rises steeply in the central $\sim 100 \text{ pc}$, and reaches to 120 km s^{-1} maximum, followed by a small dip at 250 pc . It then rises to a maximum velocity of 190 km s^{-1} at $r \sim 900 \text{ pc}$, and declines to 150 km s^{-1} at 1.5 kpc . This maximum may be due to the central bulge. Then, the rotation velocity gradually increases, representing the disk component. The small-scale fluctuation of amplitudes by $\sim \pm 10 \text{ km s}^{-1}$ may not be real

and, hence, the small local dips should not be taken seriously.

The dynamical mass in the central 100 pc is $3 \times 10^8 M_\odot$ for a rotation velocity of 120 km s^{-1} , and the mass within 1 kpc is $7 \times 10^9 M_\odot$ for 180 km s^{-1} . The high central velocity and massive core within the 100 pc region of the nucleus was observed for many galaxies (Takamiya, Sofue 2000; Sofue et al. 2001; Koda et al. 2002).

We calculated the surface-mass distributions (SMD) using the observed rotation curve by applying a deconvolution method described in Takamiya and Sofue (2000). Figure 9b shows the derived mass distributions, where the dashed line was calculated by a spherical-symmetry assumption, and the

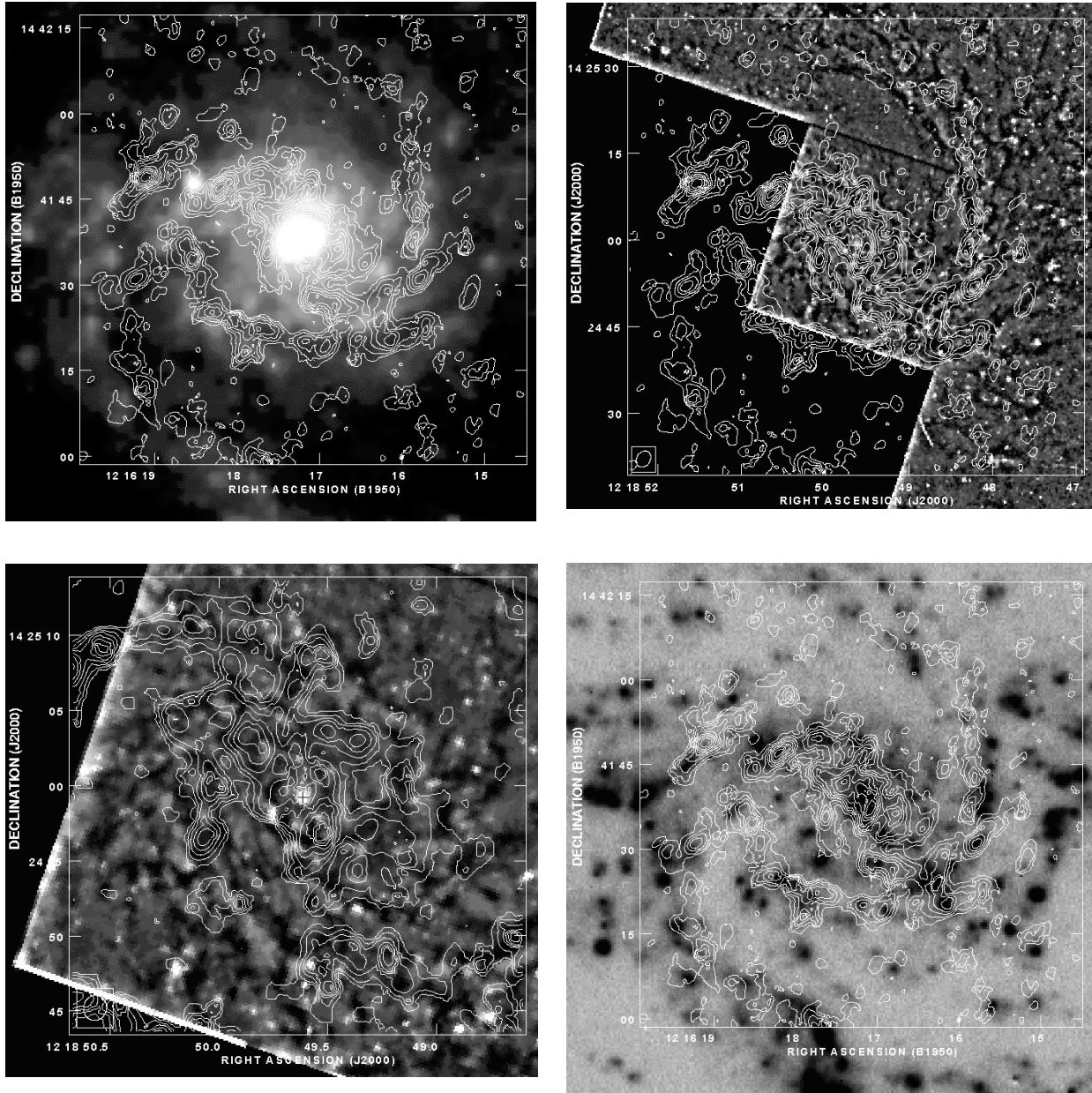


Fig. 6. (a) (Top left:) Overlay of the integrated CO intensity map, same as figure 5a, on an *R*-band negative image of NGC 4254 reproduced from Frei et al.'s (1996) galaxy catalog. (b) (Top right:) Overlay of the integrated CO intensity map, same as figure 5a, on the *B*-band positive image of NGC 4254, as reproduced from the galaxy-image archive of the Hubble-Space-Telescope. (c) (Bottom left:) The same as figure 6a, but enlarged for the central part. (d) (Bottom right:) The same as figure 6a, but overlaid on an $H\alpha$ image from Banfi et al. (1993) taken from the NED archive.

full line by a flat-disk assumption. Since the rotation curve is given only within 3 kpc, the results beyond 2.5 kpc are not real. Both the dashed and full-line results agree with each other, except for the larger fluctuations and slightly larger values for the spherical assumption. The figure indicates a high-density central peak, representing the massive core of scale radius of 80 pc with the central value being as high as $SMD = (2-3) \times 10^4 M_{\odot} \text{pc}^{-2}$. Since the values are resolution-limited, the real core radius would be smaller and the density would be higher. The massive core is followed by an exponentially decreasing part at $r \sim 0.2-1$ kpc with a scale radius of 600 pc, likely representing the bulge component. Beyond 1 kpc, the

SMD decreases more slowly, representing an exponential disk component of the scale radius of about 3 kpc, though the accuracy is much poorer for this component, because of the small radius of deconvolution.

4.2. Molecular Gas Mass

The total CO luminosity mass within the inner $22''.5$ radius region is estimated to be $2.4 \times 10^8 M_{\odot}$, using a conversion factor of $C = 2.1 \times 10^{20} \text{ cm}^{-2} \text{ K}^{-1} \text{ km}^{-1} \text{ s}$ (Arimoto et al. 1996). Taking into account the missing flux of our NMA observation and that the mass of molecular contents including He and other elements is $M_{\text{gas}} = 1.36 M_{\text{H}_2}$, the total mass of molecular gas is

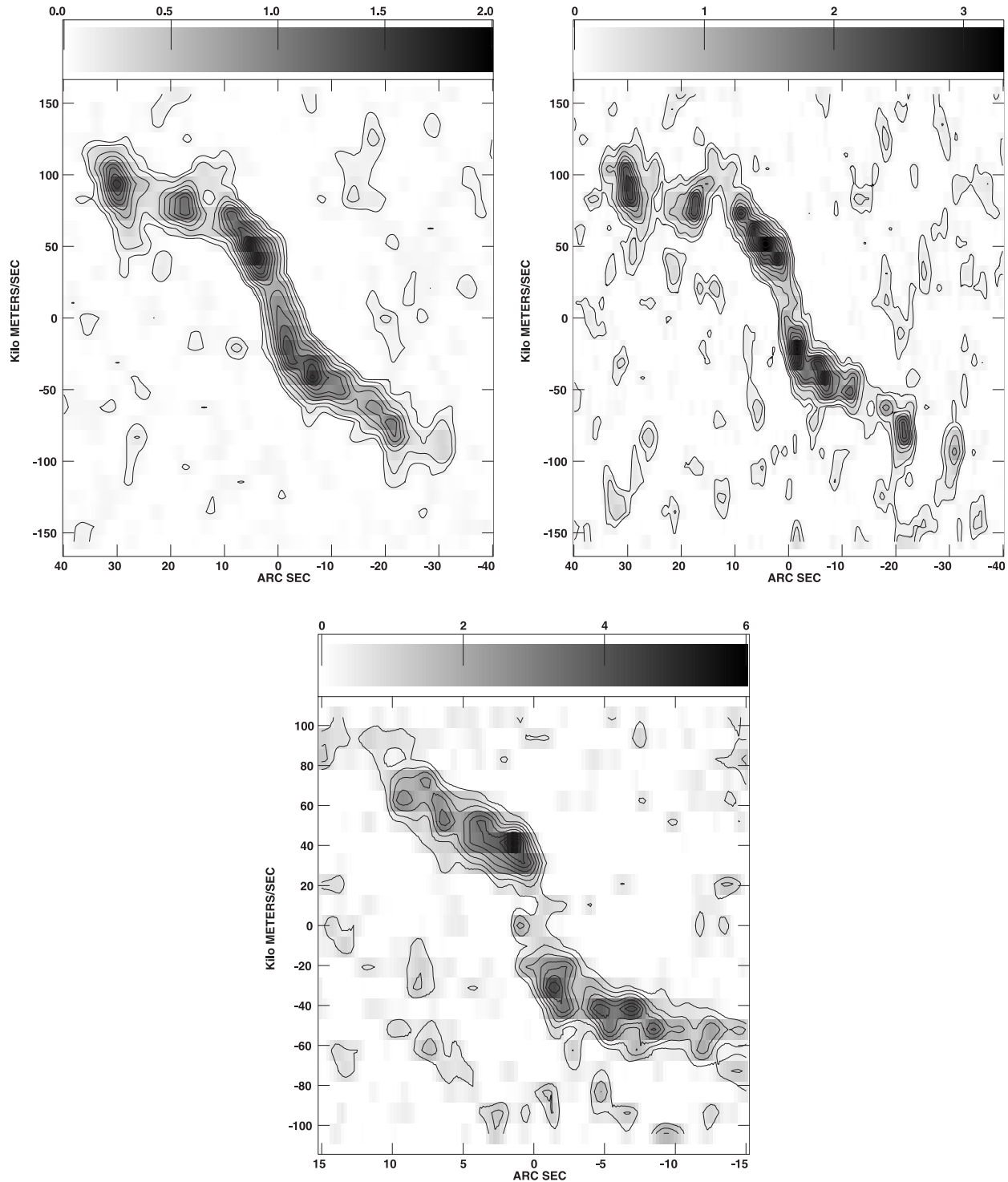


Fig. 7. (a) (Top left:) Position–velocity diagram of the CO emission in NGC 4254 from the tapered cube ($5''.22 \times 3''.45$ beam, velocity resolution 21 km s^{-1}) along a $10''$ -width slit on the major axis (P.A. = 68°) across the kinematical center. the contour levels are at 5, 10, 20, ..., 100% of the peak value of 1.73 K ($0.349 \text{ Jy beam}^{-1}$). The velocity centroid is 2402.6 km s^{-1} . (b) (Top right:) Same as figure 7a, but for natural weighting and a non-tapered cube ($2''.99 \times 2''.34$ beam, and velocity resolution 21 km s^{-1}) along a $3''$ -width slit on the major axis. The contour levels are at 5, 10, 20, 30, ..., 100% of the peak value of 3.23 K ($0.248 \text{ Jy beam}^{-1}$). (c) (Bottom:) Same as figure 7a, but for the central part from the high-resolution cube ($1''.68 \times 1''.53$ beam, and velocity resolution of 10.4 km s^{-1}) in a $2''$ -width slit along the major axis. The contour levels are every 10% of the peak value of 5.46 K ($0.152 \text{ Jy beam}^{-1}$).

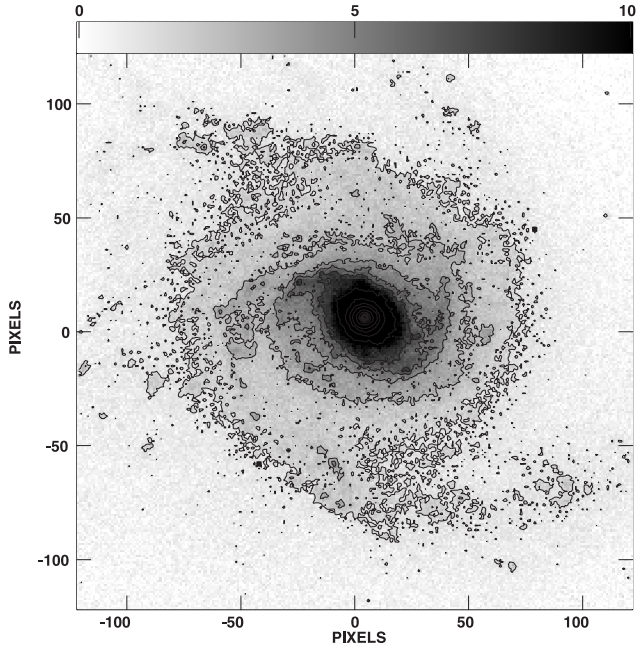


Fig. 8. *K*-band image of NGC 4254 in a contour form, taken from the NED archive of the NIR survey of nearby galaxies by Mölenhoff and Heidt (2001). The displayed area is $4' \times 4'$ around the nucleus, and 1 pixel corresponds to $1''$. The contours are drawn at 2, 4, ..., 12, 15, 20, ..., 30, 40, ..., 100% of the peak value of $7.34 \text{ DN pixel}^{-1}$.

calculated to be $4.3 \times 10^8 M_{\odot}$. The CO luminosity mass within the inner $5''$ radius region, where a missing flux correction is not needed, is $4.0 \times 10^7 M_{\odot}$. The luminosity mass to dynamical mass ratio in the inner $5''$ is 0.15, much larger than that in the inner $22''$, where the ratio is 0.026. If we adopt a more face-on value for the inclination, e.g. 29° , the above ratios should be decreased by a factor of 0.52. Hence, the molecular-gas mass in NGC 4254 is not particularly large compared with the dynamical mass.

4.3. Origin of the North–South Asymmetry in CO

Environmental effects, such as the tidal interaction and/or the ram-pressure effects, are an interesting subject concerning the Virgo galaxies. NGC 4254, which is apparently not associated with a companion galaxy, is known for its distorted HI structure, and the lopsidedness is supposed to be the result of an environmental effect due to the ram pressure by the intracluster medium (Phookun et al. 1993). The outer HI gas is largely extended in the northeastern area over $2''$ ($\sim 10 \text{ kpc}$), and is associated with several bifurcated optical arms. One prominent optical/HI arm extends from the south-to-western region; this prominent one-armed feature leads to the $m = 1$ mode based on a spiral mode analysis (Iye et al. 1982).

It was long believed that the inner disks are stable and not disturbed by such an environmental effect as the ram pressure (Vollmer et al. 2001). However, simulations have already shown that the ram effect is significant, even on the inner disks (Sofue 1994). Recently, we examined the ram effect on the inner molecular disk in detail, and showed that it is significant when it acts on the inter-arm regions, where the gas density is much lower than in the arm regions, and hence

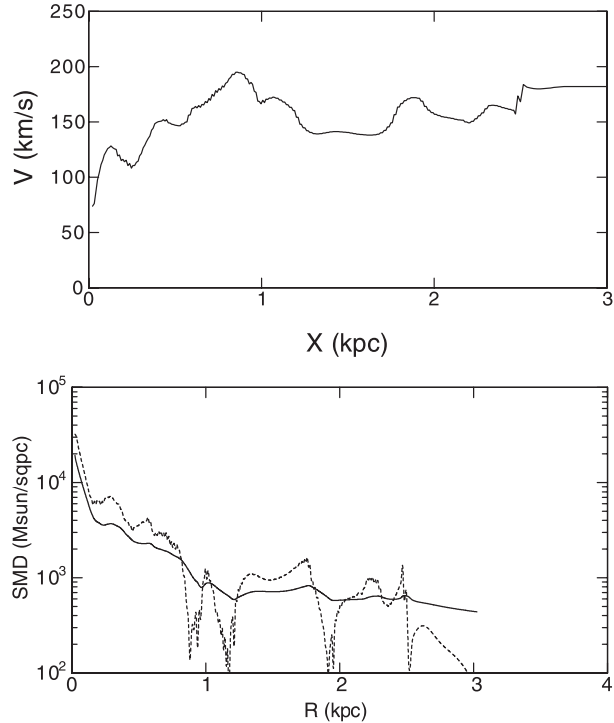


Fig. 9. (a) (Upper:) Rotation curve for the inner 3 kpc of NGC 4254 obtained by the iteration method using the PV diagram, as described in Takamiya and Sofue (2002) and Sofue et al. (2003b). (b) (Lower:) Surface-mass distribution (SMD) obtained by deconvolution of the rotation curve using the method described in Takamiya and Sofue (2000). The full line represents the result for a flat-disk assumption, and the dotted line for a spherical-symmetry assumption of the mass distribution. Note the three components: the central massive core at 0–100 pc with a scale radius of 80 pc, a bulge at 0.1–1 kpc, and the disk component at 1 to 2.5 kpc.

the ram-pressure easily disturbs the orbits of the inter-arm gas (Hidaka, Sofue 2002). The disturbed orbits of inter-arm gas leads to a significant displacement of the shocked arms from the regular bisymmetric arm positions, resulting in distorted inner molecular spiral structures. Figures 10a (top right) and 10b (top left) show the result of our two-dimensional hydrodynamical simulation of ram pressure on a gas disk with spiral arms. Here, the intracluster wind blows from the west toward the east at an inflowing angle of 45° to the galactic plane with a wind velocity of 1000 and 1500 km s^{-1} , respectively, and the ICM density is assumed to be $5 \times 10^{-4} \text{ H cm}^{-3}$. A detailed description of the model and simulation procedure is given in Hidaka and Sofue (2002).

The simulation may be compared with the observed CO intensity distribution, shown in figure 10c (bottom), the same as figure 4a. The distribution of molecular gas in the central $1'$ region of NGC 4254 is extended to the south-eastern half, where the tightly wound CO arm is most prominent. This tight arm winds out to the north, followed by the NE optical outer arms. The western arm winds out to the south, and continues to the optical/HI one-armed spiral arm. These asymmetric arm structures, particularly the tight CO arm (Arm III), are well mimicked by the simulation in figures 10a and b, although the details are not necessarily reproduced.

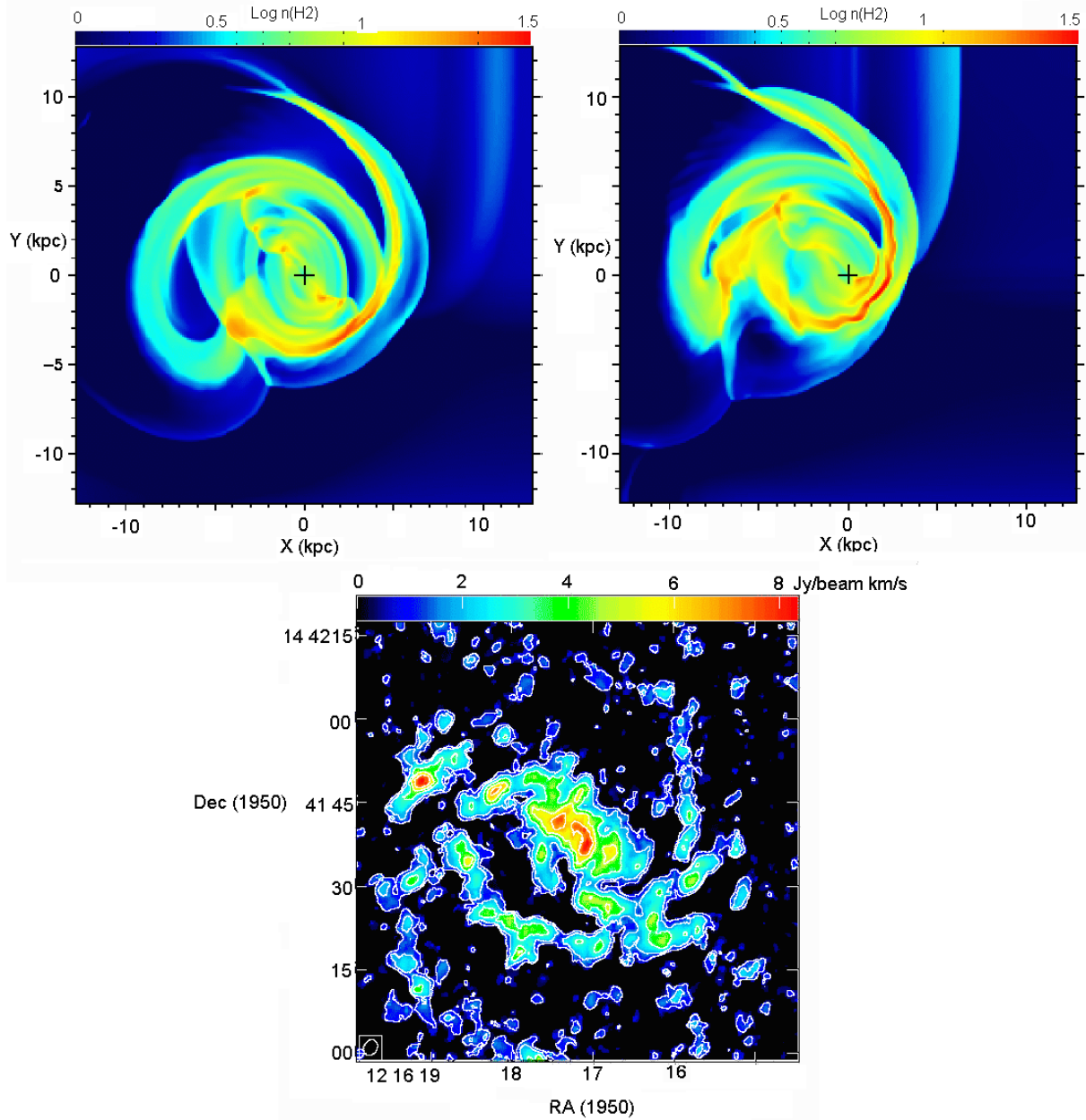


Fig. 10. Two-dimensional hydrodynamical simulation of the effect of ram pressure by an intracluster wind on the inner part of a spiral galaxy (Hidaka, Sofue 2002). (a) (Top left:) A wind with a gas density of $5 \times 10^{-4} \text{ H cm}^{-3}$ blows from the west (right) to east (left) at an inflowing angle of 45° with a wind velocity of 1000 km s^{-1} . The rotation of the galaxy is anticlockwise, just like NGC 4254. Note that the faint outer features are artifact due to an edge-reflection effect in the calculation. (b) (Top right:) The same, but with a wind velocity of 1500 km s^{-1} . (c) (Bottom:) Observed CO intensity distribution in NGC 4254 (same as figure 4a).

We are grateful to the staff at NRO for their helpful discussion about the observation and reduction. The optical images were taken via the NASA Extragalactic Data Archive (NED), and from the Hubble-Space-Telescope Data Archive at STScI

operated by NASA. J.K. was financially supported by the JSPS (Japan Society for the Promotion of Science) for young scientists.

References

- Arimoto, N., Sofue, Y., & Tsujimoto, T. 1996, PASJ, 48, 275
 Banfi, M., Rampazzo, R., Chincarini, G., & Henry, R. B. C. 1993, A&A, 280, 373
 Condon, J. J., Helou, G., Sanders, D. B., & Soifer, B. T. 1990, ApJS, 73, 359

- de Vaucouleurs, G., de Vaucouleurs, A., Corwin, H. G., Jr., Buta, R. J., Paturel, G., & Fouqué, P. 1991, *Third Reference Catalog of Bright Galaxies* (New York: Springer-Verlag)
- Ferrarese, L., et al. 1996, *ApJ*, 464, 568
- Frei, Z., Guhathakurta, P., Gunn, J. E., & Tyson, J. A. 1996, *AJ*, 111, 174
- González, R. A., & Graham, J. R. 1996, *ApJ*, 460, 651
- Hidaka, M., & Sofue, Y. 2002, *PASJ*, 54, 33
- Iye, M., Okamura, S., Hamabe, M., & Watanabe, M. 1982, *ApJ*, 256, 103
- Kenney, J. D., & Young, J. S. 1988, *ApJS*, 66, 261
- Koda, J., Sofue, Y., Kohno, K., Nakanishi, H., Onodera, S., Okumura, S. K., & Irwin, J. A. 2002, *ApJ*, 573, 105
- Möllenhoff, C., & Heidt, J. 2001, *A&A*, 368, 16
- Okumura, S. K., et al. 2000, *PASJ*, 52, 393
- Phookun, B., Vogel, S. N., & Mundy, L. G. 1993, *ApJ*, 418, 113
- Sakamoto, K., Okumura, S. K., Ishizuki, S., & Scoville, N. Z. 1999, *ApJS*, 124, 403
- Schöniger, F., & Sofue, Y. 1997, *A&A*, 323, 14
- Sofue, Y. 1994, *ApJ*, 423, 207
- Sofue, Y., Koda, J., Kohno, K., Okumura, S. K., Honma, M., Kawamura, A., & Irwin, J. A. 2001, *ApJ*, 547, L115
- Sofue, Y., Koda, J., Nakanishi, H., & Onodera, S. 2003b, *PASJ*, 55, 59
- Sofue, Y., Koda, J., Nakanishi, H., Onodera, S., Kohno, K., Tomita, A., & Okumura, S. K. 2003a, *PASJ*, 55, 17
- Soifer, B. T., Sanders, D. B., Madore, B. F., Neugebauer, G., Danielson, G. E., Elias, J. H., Lonsdale, C. J., & Rice, W. L. 1987, *ApJ*, 320, 238
- Takamiya, T., & Sofue, Y. 2000, *ApJ*, 534, 670
- Takamiya, T., & Sofue, Y. 2002, *ApJ*, 576, L15
- Vollmer, B., Cayatte, V., Balkowski, C., & Duschl, W. J. 2001, *ApJ*, 561, 708
- Yasuda, N., Okamura, S., & Fukugita, M. 1995, *ApJS*, 96, 359